Journal of Orthopaedic Translation 49 (2024) 218–229

Contents lists available at ScienceDirect

Journal of Orthopaedic Translation

journal homepage: www.journals.elsevier.com/journal-of-orthopaedic-translation

Original Article

Engineering natural DNA matrices with halloysite nanotubes to fabricate injectable therapeutic hydrogels for bone regeneration

Yali Miao [a,b,1], Teliang Lu [a,b,1], Shangbin Cui [d,1], Ziyang Xu [a,b], Xiao Liu [c,*], Yu Zhang [a,b,**]

[a] Guangdong Cardiovascular Institute, Guangdong Provincial People's Hospital, Guangdong Academy of Medical Sciences, 510080, China
[b] Department of Orthopedics, Guangdong Provincial People's Hospital, Guangdong Academy of Medical Sciences, Guangzhou, Guangdong, 510080, China
[c] Greater Bay Area Institute for Innovation, Hunan University, Guangzhou, Guangdong, 511300, China
[d] Guangdong Provincial Key Laboratory of Orthopaedics and Traumatology, Department of Spinal Surgery, the First Affiliated Hospital of Sun Yat-sen University, Guangzhou, Guangdong, 510080, China

ARTICLE INFO

Keywords:
Bone regeneration
DNA
Drug delivery
Halloysite nanotubes
Injectable hydrogels
Nanocomposites

ABSTRACT

Background: Injectable hydrogels are widely used in drug delivery and the repair of irregular tissue defects due to their advantages such as convenient and minimally invasive operation. Although the existing injectable hydrogels have excellent biocompatibility and osteoconduction, they still face clinical challenges such as low osteogenic activity. The key requirements for improved injectable hydrogels as repair materials for non-load bearing bone defects are optimal handling properties, the ability to fill irregular defects and provide osteoinductive stimulation.

Methods: We developed an approach to construct injectable hydrogels through a two-step gelation process. In the first step of gelation, the denaturation and rehybridization mechanism of natural biopolymer DNA was utilized to form interconnected structure through hydrogen bonding between complementary base pairs between the DNA strands. In the second step of gelation, the introduction of halloysite nanotubes (HNTs) loaded with osteogenic model drug dexamethasone (Dex) provided additional crosslinking sites through non-covalent interactions with the DNA backbone, including electrostatic interaction and hydrogen bonding interaction.

Results: The DNA-based nanocomposite hydrogel material developed in our work can be used as an injectable filling material for the repair of non-load bearing bone defect and can be loaded with osteogenic model drug dexamethasone (Dex) for improved osteoinductivity, promoting new bone regeneration *in vivo*.

Translational potential of this article: This article highlights the potential of using nanocomposite hydrogels to repair non-load bearing bone defects, which are common injuries in the clinic. This study provides a deeper understanding of how to optimize the properties of hydrogels to regulate cell differentiation and tissue formation.

1. Introduction

Injectable physical crosslinked hydrogels have a three-dimensional network in which polymer chains are bound together through non-covalent interactions including hydrophobic interactions, hydrogen bonding interactions, and electrostatic interactions [1–3]. The main advantage of physical cross-linked hydrogels is that toxic crosslinking agents are not required during preparation, which may lead to problems with biocompatibility or hinder the bioactivity of biomolecules inside. Physical cross-linked hydrogels exhibiting shear-thinning behavior can be easily administered *via* medical syringe due to their ability to reassemble after the removal of shear forces. Therefore, injectable physical crosslinked hydrogels have obvious advantages in the field of bioactive molecular delivery and repair of irregular bone defects [4–6]. Current treatment for bone defects heavily relies on invasive surgery, where materials are surgically implanted into the bone defect site. The emergence of injectable hydrogels provides a new idea for the treatment of bone defects, which can be then directly injected into the defect site and

* Corresponding author.
** Corresponding author. Guangdong Cardiovascular Institute, Guangdong Provincial People's Hospital, Guangdong Academy of Medical Sciences, 510080, China.
E-mail addresses: 497216514@qq.com (X. Liu), luck_2001@126.com (Y. Zhang).
[1] Yali Miao, Teliang Lu, and Shangbin Cui contributed equally to this work.

https://doi.org/10.1016/j.jot.2024.09.010
Received 4 June 2024; Received in revised form 8 September 2024; Accepted 25 September 2024

delivered with therapeutic drugs *via* minimally invasive injection [7–10]. From a clinical perspective, minimally invasive surgery reduces the risk of infection and minimizes postoperative scar formation.

Natural biopolymers are high molecular weight compounds obtained from animal and plant sources, including proteins, polysaccharides, and nucleic acids, which have good biocompatibility and biodegradability [11–13]. Natural polymers are widely used in the preparation of hydrogels because of their superior biocompatibility than synthetic polymers. However, in most cases, natural polymers require additional functionalization steps or introduction of other polymers to provide the reactive structural unit for crosslinking [14,15]. Recently, a more effective strategy to construct injectable hydrogels is to use the self-assembly process between polymers with specific molecular recognition motifs to obtain hydrogels with injectable properties [16,17]. As a natural polymer, DNA has a high degree of specificity between its base pairs and can form a double helical structure, thus spontaneously forming a supramolecular physical cross-linking network [18,19]. Moreover, DNA molecular chains have modifiable sites that can chemically and physically bind to other bioactive substances. Therefore, treating DNA as a natural polymer rather than a genetic material has great potential in the field of hydrogel application [20–22]. Currently, the crosslinking mechanisms of DNA hydrogels include enzyme-mediated reactions, covalent bonding interactions, and complementary base pairing, etc [23]. However, only a few studies have reported on the possibility of forming injectable hydrogels by using non-covalent interactions between the DNA intrinsic bases [24].

Recent studies have shown that halloysite nanotubes (HNTs) can enhance the strength of the crosslinking network through non-covalent interactions with polymers [25,26]. HNTs are also one of silicates, with the chemical formula of $Al_2Si_2O_5(OH)_4{\cdot}nH_2O$. As the natural nanomaterial with tubular structure, HNTs have the structure similar to carbon nanotubes. The inner and outer surfaces of HNTs have different electrical properties, with an aspect ratio of 10–30. In addition, HNTs have good adsorption properties, mechanical properties and biocompatibility, which have attracted the attention of many researchers [26–28]. Higher aspect ratio can reduce the contact area between the HNTs, so that the HNTs can be effectively and uniformly dispersed in other composites [29–31]. Theoretically, the active hydroxyl groups of HNTs enable hydrogen bonding interactions with the amino or hydroxyl groups on the polymer chains to prepare hydrogels [32]. The reversibility of the hydrogen bond allows for the recovery of the strain modulus immediately after the hydrogel injection and improves the mechanical strength of the hydrogels [33,34]. Therefore, HNTs may also serve as ideal candidates for injectable hydrogel design. According to the above characteristics, HNTs are often used to design drug delivery systems to regulate the release of bioactive substances, including drugs, growth factors, and vaccines [35,36].

Herein, we reported the formation of injectable hydrogels based on DNA and HNTs, which can be prepared by high-temperature denaturation and low-temperature rehybridization mechanisms of DNA, and the physical mixing technique of HNTs. The advantage of this strategy was the development of physical crosslinked network without chemical modifications or the design of specific base sequences. The prepared hydrogel consisted of two different types of network points: the formation of the DNA chains caused by the heating step and the non-covalent interaction of HNTs with the DNA backbone. We investigated the effects of HNTs on the rheological behavior of the hydrogel, including shear thinning and injectability. Furthermore, the interactions between HNTs and the DNA network were analyzed by X-ray photoelectron spectroscopy (XPS). As a proof of concept, we examined *in vitro* the ability of the constructed nanocomposite hydrogel system to regulate the release of the osteogenic model drug dexamethasone (Dex). We expected that the designed injectable DNA nanocomposite hydrogels have broad applications in biomedical field, such as tissue regeneration, drug carriers, bioinks.

2. Materials and methods

2.1. Preparation of the nanocomposite hydrogel

To prepare the nanocomposite hydrogel, DNA (D1626, Sigma–Aldrich, USA, molecular weight ~1.3×10^6 g/mol) at a concentration of 4 w/v% was first dispersed in ultrapure water and stirred for 6 h at 45 °C until the DNA was completely dissolved. Then, halloysite nanotubes (HNTs, 103763, Nanjing XFNANO Materials Tech Co., Ltd, China) were added to the DNA solution, the final concentration of HNTs in the solution was 3 wt%. The mixture was magnetically stirred for 1 h to unify the HNTs in the DNA solution. Further, the mixture was heated at 95 °C for 2 min. After that, the heated mixture was cooled at room temperature for 15 min and stored at 4 °C overnight to complete the final gelation.

DNA-based hydrogels can be used as injectable hydrogels for minimally invasive treatment but also as delivery carriers. In order to verify this concept, we selected the osteogenic model drug dexamethasone (Dex, D4902, Sigma–Aldrich, USA) to load on the DNA-HNTs hydrogel. The HNTs loaded with the Dex were performed as described by other research groups [26,35]. Briefly, the Dex powder was dissolved in anhydrous ethanol to obtain a 20 w/v% Dex solution. Then, 4 g HNTs and 30 mL of Dex solution were mixed, vortexed for 30 s and sonicated for 2 h. After the mixture was vacuum, centrifuged, and completely dried, the Dex-loaded HNTs were obtained for further use. The drug entrapment efficiency (E.E) of HNTs was calculated as E.E (%) $=([Dex]_{total}\text{-}[Dex]_{free})/[Dex]_{total} \times 100$ %. Specifically, $[Dex]_{total}$ and $[Dex]_{free}$ were the amount of total drug added during the preparation process of the HNTs loaded with the Dex and the final remaining amount of free drug, respectively. Finally, the obtained Dex-loaded HNTs were added to the DNA pre-gel to obtain the DNA-HNTs + Dex hydrogel. In addition, we also set up a group of DNA hydrogel directly loaded with Dex for release study, and the concentration of Dex remained unchanged.

2.2. Internal morphology and molecular interactions of DNA-based hydrogels

To investigate the binding ability between DNA and HNTs, DNA was mixed with HNTs dispersion, and the mixture was washed and centrifuged to obtain the HNTs with adsorbed DNA, labeled as DNA@HNTs. The particle size distribution and surface potential of HNTs were measured by a Zetasizer instrument (Nano ZS90, Malvern, UK). The HNTs and DNA@HNTs dispersion were separately diluted to appropriate concentrations and characterized by using Transmission Electron Microscopy (TEM, JEM-2100HR, JEOL, Japan).

In order to characterize the influence of HNTs on the internal topography of DNA hydrogel, freeze-dried hydrogels were pasted onto the sample stage with conductive adhesive and observed by using Scanning Electron Microscopy (SEM, MERLIN, Zeiss, Germany) at an accelerating voltage of 1–10 kV. The pore size of each group was analyzed from five different images by using ImageJ software. To further study the influence of the introduction of HNTs on the degradation behavior of hydrogels, the freeze-dried hydrogels were weighed (W_0) and placed in centrifuge tubes. After that, the hydrogels of different groups were immersed in PBS (0.02 g/1 mL) at 37 °C and exposed to DNase (1 U/mg DNA), respectively. At the set time points, the hydrogels were collected by centrifugation, and weighed (W_t) after freeze-drying. The degradation rate (DR) of the hydrogels were calculated as DR (%)$=(W_0\text{-}W_t)/W_0 \times 100$ %. Fourier Infrared Spectrophotometer (FTIR, CCR-1, Thermo Scientific, USA) was used to obtain the FTIR spectra of the hydrogels to analyze the interactions between HNTs and DNA molecular chains. The freeze-dried samples were mixed with KBr and compressed into sheets for recording spectra in the range of 400–4000 cm^{-1} with a resolution of 1 cm^{-1}.

We used the Thermo Scientific Escalab 250Xi optoelectronic

Spectrometer (XPS) to analyze the interactions between the HNTs inside the hydrogel and the DNA chain segment. Freeze-dried samples were used for all test samples. All tests used a monochrome Al Kα ($h\nu$ = 1486.6 eV) radiation source, with a 650 μm X-ray beam. We used pass energy (PE) of 150 eV, energy step size of 1 eV to record the full XPS spectra of DNA and DNA-HNTs hydrogels, and further used pass energy of 30 eV, energy step size of 0.05 eV to record high-resolution spectra of O 1s, N 1s and P 2p for DNA and DNA-HNTs hydrogels. All data were processed by using the Thermo Avantage software.

2.3. Rheological analysis

The rheological analysis was performed by Oscillating Rheometer (MCR 302, Anton Paar, Austria). Viscosity measurements were conducted at 25 °C with a shear rate range of 0.001–1000 s^{-1}. Frequency sweep meaurements were performed for all samples in the range of 0.01 Hz–100 Hz at 1 % strain. Temperature sweep experiments were performed at a frequency of 1 Hz in the range of 25–45 °C, with the temperature increasing at a rate of 1 °C/min. For the self-healing property measurements, continuous step change of oscillatory strain between 100 % and 1 % at 1 Hz was applied to test the strain-induced destruction and recovery of DNA-HNTs hydrogel.

2.4. In vitro dexamethasone release studies

Drug release studies were performed by using the Slide-A-Lyzer ™ mini-dialysis cup (MWCO: 2 kDa, Thermo Scientific™, USA). Each dialysis cup was filled with 300 μL hydrogel and the experiment was performed in 48-well plates containing 600 μL DPBS and placed in shaking incubators at the condition of 37 °C and 100 rpm. Release medium was collected at the set time points and the absorbance of medium was measured by using a microplate reader (Thermo 3001, Thermo Scientific, USA) at the wavelength of 240 nm. In order to avoid the interference of hydrogel degradation products on the absorbance of Dex, the absorbance of the release medium of DNA hydrogel and DNA-HNTs hydrogel was used as the blank group to normalize the absorbance of the release medium of DNA + Dex hydrogel and DNA-HNTs + Dex hydrogel respectively. A standard curve of Dex in the range of 0.01–0.5 mg/mL was used to quantify the amount of Dex released.

2.5. In vitro cell compatibility

DNA-based nanocomposite hydrogels have the potential as injectable tissue repair materials and drug carriers, which are expected to achieve continuous release of therapeutic agents. To evaluate the retention of the activity of the Dex inside the hydrogel, we investigated the effects of nanocomposite hydrogel loaded with the model drug Dex on the behavior of cell proliferation and osteogenic differentiation. Mouse bone mesenchymal stem cells (mBMSCs, ATCC, CRL-12424, USA) were cultured in Dulbecco's modified Eagle medium (DMEM, C11995500BT, Gibco, USA) containing 10 % fetal bovine serum (FBS, C2027050, Gibco, USA) and 1 % penicillinstreptomycin (15140-122, Gibco, USA). BMSCs were cultured at 37 °C under 5 % CO_2. All experiments were performed by using cells from passages 3 to 5. To assess the biocompatibility of the hydrogels, we first dispersed the hydrogel in complete medium (200 μL hydrogel/2 mL complete medium), and then BMSCs were cultured in 48-well plates until cell adhesion and exposed to different nanocomposite hydrogel formulations. Subsequently, cell proliferation was monitored by Cell Counting Kit-8 (CCK-8) assay and live-dead staining after 1, 3, and 5 days of exposure to the nanocomposite system. Live cells were stained with Calcein-AM (17783, Sigma–Aldrich, USA) as green, whereas the dead cells were stained with ethidium homodimer-1 (E1903, Sigma–Aldrich, USA) as red.

2.6. In vitro osteogenic differentiation

5×10^4 BMSCs were seeded in 48-well plates and cultured in complete medium until cell adhesion and then exposed to different nanocomposite hydrogel formulations. The culture medium of each group in the well plate was changed every other day. On day 7, Alkaline phosphatase (ALP) generated by BMSCs was detected by using Alkaline Phosphatase Color Development Kit (C3206, Beyotime Biotechnology, China). The ALP activity of the cells was further determined by using Alkaline Phosphatase Assay Kit (P0321, Beyotime Biotechnology, China). After the BMSCs were exposed to different hydrogel formulations for 14 days, the formation of the cell mineralized matrix was visualized by Alizarin Red staining. 0.2 % Alizarin Red S Staining Solution (C0140, Beyotime Biotechnology, China) was added to the well plate for 10 min, and the floating color was washed with DPBS for several times to remove it. After drying, it was photographed and observed under a light microscope. To quantify the formation of cell mineralized matrix, 200 μL of configured 100 mM dodecylpyridine chloride solution was added to the stained samples in the well plates. After 1 h of incubation at room temperature, 110 μL of the incubation solution was absorbed into a new 96-well plate, and the OD values of the samples were measured at the wavelength of 562 nm by using a microplate reader.

The expression levels of osteogenesis-related genes were analyzed by fluorescence real-time quantitative reaction (qRT-PCR). The mRNA was extracted for each sample after exposing the cells to different hydrogel formulations for 7 and 14 days. GAPDH as the house-keeping gene was used to determine the expression levels of Runt-related transcription factor-2 (Runx-2), Alkaline phosphatase (ALP), Collagen I (Col-I), Bone sialoprotein (BSP), and Osteocalcin (OCN). The relative fold of gene expression was calculated by using the ΔΔCt method. Experimental results were normalized according to the gene expression levels of BMSCs cultured in complete medium.

2.7. In vivo bone repair properties of injectable nanocomposite hydrogel

The animal surgeries for *in vivo* experiments were performed at the Guangzhou Seyotin Technology Co., Ltd. All experimental procedures with animals were approved by the Animal Care and Use Committee (No. SYT2024038). All surgical procedures were performed under sterile conditions. *In vivo* bone repair performance of a nanocomposite hydrogel loading the model drug Dex was evaluated by the cranial defect of Sprague Dawley rat (SD, 6 weeks, female). 2 wt% sodium pentobarbital solution was filtered and then injected intraperitoneally into rats at a dose of 1.5 mL/100 g. After anesthesia, the rat cranial area was disinfected and circular holes (d = 5 mm) were drilled on both sides of the cranium. The DNA hydrogel, DNA-HNTs hydrogel or DNA-HNTs + Dex hydrogel was randomly injected into the defect site, and the group without the injected material was considered as blank group. Rats were sacrificed at the set time points and the removed cranial tissues were fixed with 4 % paraformaldehyde solution. Then, the isolated cranial defect was scanned by using the Micro-CT analysis system (Explore Locus SP, GE, USA), and finally the relevant bone parameters based on the Micro-CT images were calculated by using ZKKS-MicroCT4.1 software. For histological morphological observation of the cranial defect, the isolated cranial tissue was decalcified, paraffin-embedded and section stained, including H&E, Masson and OCN immunohistochemical staining.

2.8. Statistical analysis

Data requiring statistical analyses were evaluated using the Prism 6 program (GraphPad Software, La Jolla, USA). All the data obtained were expressed as means ± standard deviation (SD) and were analyzed using one-way ANOVA with a post hoc test. Differences between the experimental and control groups were compared. Groups with $p < 0.05$ were

marked as significantly different (*$p < 0.05$, **$p < 0.01$, ***$p < 0.001$).

3. Results and discussion

3.1. Injectable nanocomposite hydrogels with porous structure

In this study, DNA was used as a natural polymer to form hydrogel. A basic structural feature of DNA is the specific base pairing interaction. Initially, we disrupted the hydrogen bonds between base pairs of the DNA backbone through heat treatment to denature the DNA double helix. The subsequent cooling process accelerated base pairing between adjacent DNA chains to randomly rehybridize, ultimately forming a three-dimensional structured injectable hydrogel matrix (Fig. 1a). To investigate the binding ability between DNA and halloysite nanotubes (HNTs), DNA was mixed with HNTs dispersion, and the mixture was washed and centrifuged to obtain the HNTs with adsorbed DNA, labeled as DNA@HNTs. As shown in the TEM images (Fig. 1b), the original HNTs displayed clear edges, while the DNA@HNTs exhibited a morphology with membrane coverage. Length analysis of the HNTs and DNA@HNTs conducted by dynamic light scattering (DLS) showed a significant increase in the average size of DNA@HNTs compared to the original HNTs (Fig. 1c–d). Additionally, the surface potential of DNA@HNTs also changed significantly (Fig. 1d). These characterization results clearly confirmed the physical interactions between DNA backbone and HNTs, so that HNTs were dispersed in a DNA solution without aggregation, further enhancing the dispersion stability of HNTs.

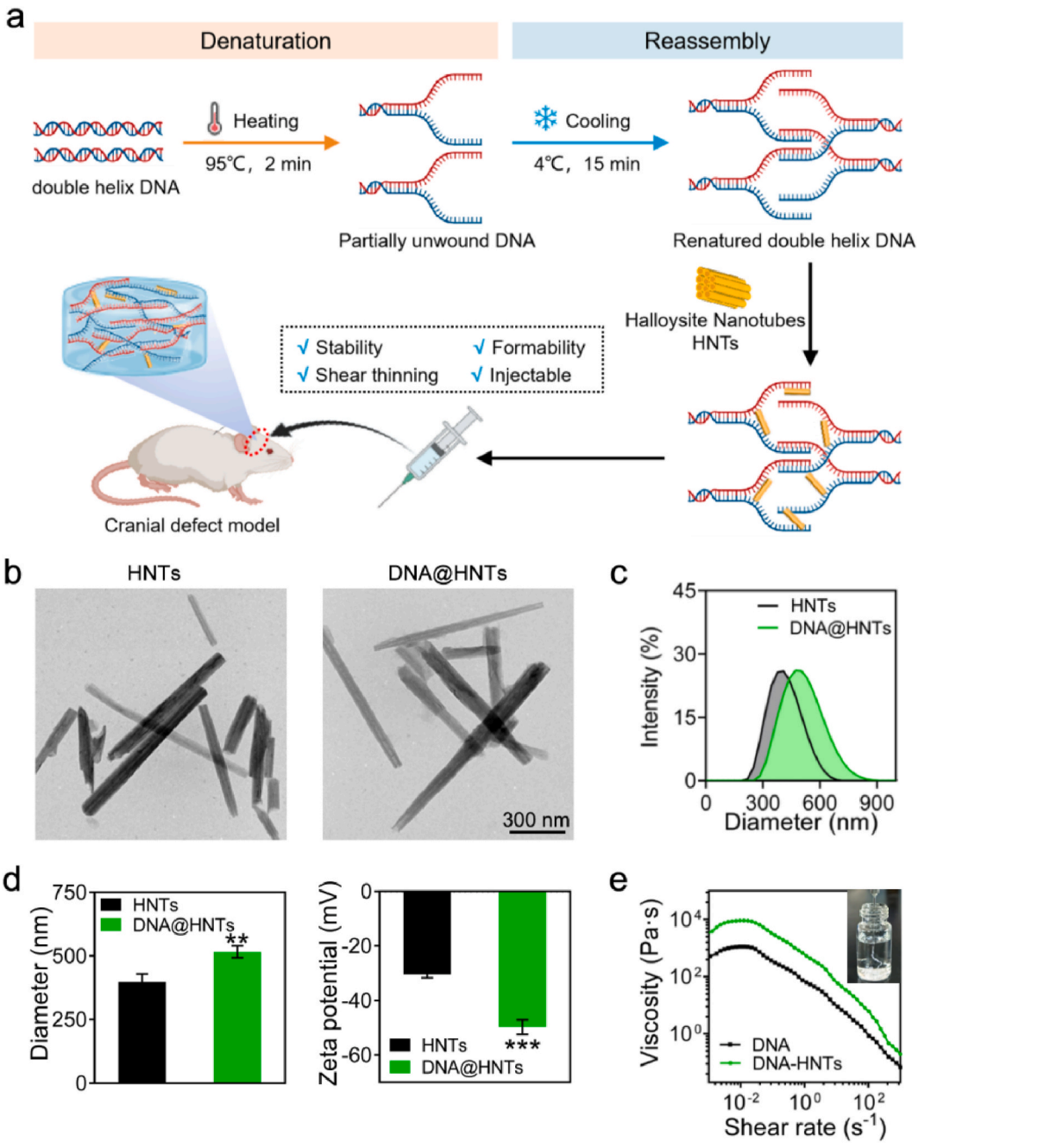

Fig. 1. (a) Schematic diagram of design strategy for developing multifunctional nanocomposite hydrogels. (b) Transmission electron microscope image of HNTs and DNA@HNTs. (c–d) Dynamic light scattering results of HNTs and DNA@HNTs: (c) particle size distribution, (d) particle size and Zeta potential. (e) The graph of viscosity-shear rate curves illustrated the increase in viscosity caused by the presence of HNTs. The hydrogels showed typical shear thinning behavior, and DNA-HNTs hydrogel can be injected by a syringe, appearing fibrous in a liquid environment. *$p < 0.05$, **$p < 0.01$, ***$p < 0.001$.

Further, high temperature triggered DNA denaturation, and low temperature drived DNA rehybridization, leading to the formation of interconnected structures. We examined the physicochemical properties of different hydrogel systems by conducting morphology detection and rheological measurements on the hydrogels. From Fig. 1e, the viscosity of DNA hydrogel decreased with the shear rate, demonstrating that DNA hydrogel can reassemble after undergoing shear forces, which was a necessary condition for injectable hydrogel. After the addition of HNTs, the nanocomposite hydrogels also showed a similar shear-thinning behavior and injectable formability. It was noteworthy that the introduction of HNTs could not affect the injectable performance of DNA hydrogel, and the injected fibers of DNA-HNTs hydrogel were also shown in Fig. 1e. From the SEM images in Fig. 2a–b, we can observe that the introduction of HNTs led to a significant reduction in the pore size of the hydrogel, illustrating that HNTs involved in the formation of the hydrogel network and led to an increase in crosslinking density.

We further conducted rheological measurement to evaluate the effect of HNTs on the mechanical properties of DNA hydrogels. The variation of the storage modulus (G′) of the hydrogels was monitored by applying two consecutive cycles of high (100 %) and low (1 %) strain (Fig. 2c). DNA-HNTs hydrogel maintained a high mechanical state under low strain conditions and exhibited a low mechanical state similar to a fluid under high strain. After returning to low strain, the hydrogel returned to its initial state and exhibited similar mechanical changes at the next test time point, indicating that the DNA-HNTs hydrogel had self-repair capabilities after high strain. Frequency sweep test was performed on the hydrogel under the condition of 1 % strain (Fig. 2d), it can be observed that the G′ value was clearly increased with the introduction of HNTs in the angular frequency range of 0.1 rad/s to 100 rad/s, and this result also confirmed the classical hydrogel behavior, as the G' values of the hydrogels were dominant across the range of low angular frequency. In addition, Tanδ values of DNA and DNA-HNTs hydrogels displayed no significant change in the temperature range of 25 °C–45 °C, indicating that the both hydrogel systems maintained their elastic performance (Fig. 2e). Based on the results of rheological measurement, it can be concluded that the introduction of HNTs effectively enhanced the strength of the DNA crosslinking network, and that the interactions between HNTs and DNA chain synergatively regulated the mechanical stability of the hydrogel.

The degradation of hydrogels is important for tissue regeneration as the generated new spaces are able to provide microenvironments that facilitate cell migration and tissue ingrowth. The degradation curves of the hydrogels were shown in Fig. 2f, revealing that the two hydrogels degraded at different rates. The slightly decreased degradation rate with HNTs incorporation might be attributed to the increase in the crosslinking densities of the composite networks. DNA-based hydrogels were further analyzed by Fourier transform infrared spectrometer (FTIR), as shown in Fig. 2g. From the FTIR spectrum, it can be seen that there was an obvious -NH_2 stretching vibration peak at 3420 cm^{-1} in the infrared spectrum of DNA hydrogel. After the HNTs were introduced, the width of the -NH_2 characteristic peak became significantly wider and moved to the low wavenumber region (3400 cm^{-1}), which was due to the hydrogen bond interaction between -OH of HNTs and -NH_2 of DNA hydrogel. In addition, we can also observe the PO^{2-} bending vibration

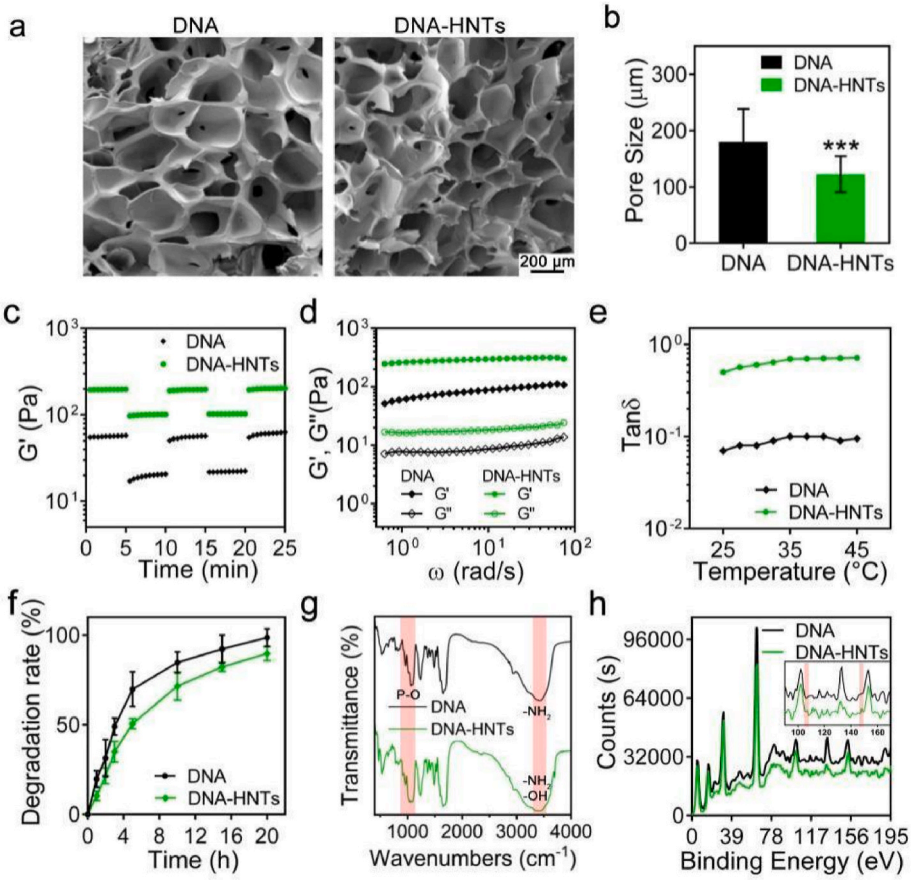

Fig. 2. (a) SEM images of DNA-based hydrogels showed porous structures (scale bar = 200 μm). (b) The pore size inside the hydrogel network was analyzed by ImageJ software, showing that the pore size of the hydrogel network was significantly reduced after the introduction of HNTs. (c–e) Rheological analysis of DNA-based hydrogels: (c) the change of G′ values under alternating high and low strain, (d) frequency sweep curves, (e) temperature sweep curves carried out from 25 °C to 45 °C. (f) Enzymatic degradation of the DNA and DNA-HNTs hydrogels. (g) FTIR spectrums of DNA hydrogel with and without HNTs. (h) XPS spectrums of DNA-based hydrogels confirmed the existence of HNTs in DNA hydrogel. *$p < 0.05$, **$p < 0.01$, ***$p < 0.001$.

peaks at 963 cm^{-1} and 1065 cm^{-1} in the infrared spectrum of DNA hydrogel, both of which represented the structural characteristic peaks of DNA. After the introduction of HNTs, there were significant changes in the shape and intensity of the PO^{2-} characteristic peak, which was speculated that this may be due to the electrostatic interaction between the PO^{2-} of DNA and the positively electric regions of the HNTs, leading to changes in the DNA molecular environment. X-ray photoelectron spectroscopy (XPS) assay further confirmed the existence of HNTs in the crosslinking network (Fig. 2h). The peaks at ~107 eV and ~148 eV corresponded to Si 2p and Si 2s of HNTs, and there was no Si 2p and Si 2s in the DNA hydrogel system, indicating that injectable nanocomposite hydrogel was successfully formed.

Furthermore, XPS studies validated the type of interactions between DNA and HNTs, and explored the function of HNTs in enhancing the DNA hydrogel network. XPS spectra were recorded to assess the differences between hydrogels with and without HNTs, including oxygen (O 1s), phosphorus (P 2p), and nitrogen (N 1s) (Fig. 3a–c). The O 1s peak of the DNA hydrogel was at ~531.24 eV, while the O 1s peak of the hydrogel containing HNTs was shifted towards a higher binding energy (~535.96 eV), indicating a change in the electronic environment near the oxygen and phosphorus. The spectrum of P 2p was divided into two spin-double states, P_1 and P_2. For DNA samples, P_1 corresponds to P $2p_{3/2}$ at ~132.31 eV, while P_2 corresponds to P $2p_{1/2}$ at ~133.28 eV (Fig. 3d), which was consistent with previous reports [37]. Specifically, the binding energy of P_1 and P_2 in the DNA-HNTs hydrogel was increased by 0.16 eV and 0.27 eV, respectively. The reason for this result was that the electrostatic attraction between the positively charged region of HNTs and the negatively charged oxygen in the phosphate group of the DNA destabilized the electronic environment around the nearest phosphorus atoms, which led to a decrease in the electron density around phosphorus, resulting in an increased binding energy. Furthermore, the O 1s spectra of the DNA-HNTs nanocomposite hydrogel showed a distinct redistribution between O_1 and O_2 (Fig. 3e). This transition was due to the electrostatic interaction of the phosphate group in DNA with the positively charged region of the HNTs, resulting in a decrease in the electron density near the O_1 site.

To verify the possibility of other interactions between HNTs and DNA bases, we compared the N 1s spectra of the two systems. Because of the different chemical environment of the nitrogen atoms, N 1s was deconvolved into two peaks, N_1 and N_2 (Fig. 3f). For the DNA sample, the N_1 peak was assigned to the nitrogen atoms of the C=N-C and C-NH_2 groups, corresponding to a binding energy of ~397.81 eV. The N_2 peak was assigned to the nitrogen atoms of the -N-C-O and -N-C=O group, corresponding to a binding energy of ~399.17 eV. The N_1 and N_2 of the DNA-HNTs hydrogel showed the change of peak shape compared with the DNA hydrogel. This transition was due to the hydrogen bonding interaction between the reactive hydroxyl groups on the surface of the HNTs and the DNA bases. Overall, the XPS results confirmed the presence of electrostatic interaction between HNTs and the oxygen atoms of the phosphate anion (PO^{2-}) in the DNA backbone, and hydrogen bonding interaction between HNTs and DNA. The XPS results described that the introduction of HNTs provided additional crosslinking sites in the preparation of the DNA hydrogel, which was the main reason for the increased mechanical strength of the DNA hydrogels.

3.2. *Activity of encapsulated drug: evaluation of osteogenic function in vitro*

DNA-based hydrogel have properties similar to the extracellular matrix, and we anticipated that this hydrogel can be used as a continuous drug delivery carrier in addition to applying minimally invasive therapy as an injection hydrogel. As a proof of concept, we encapsulated an osteogenic model drug dexamethasone (Dex) in a hydrogel and monitored its release over a period of 12 days *in vitro*. Specifically, the Dex loading efficiency of HNTs was about 49.7 %. Dex is a well-known osteogenic drug that can stimulate osteogenic differentiation of stem

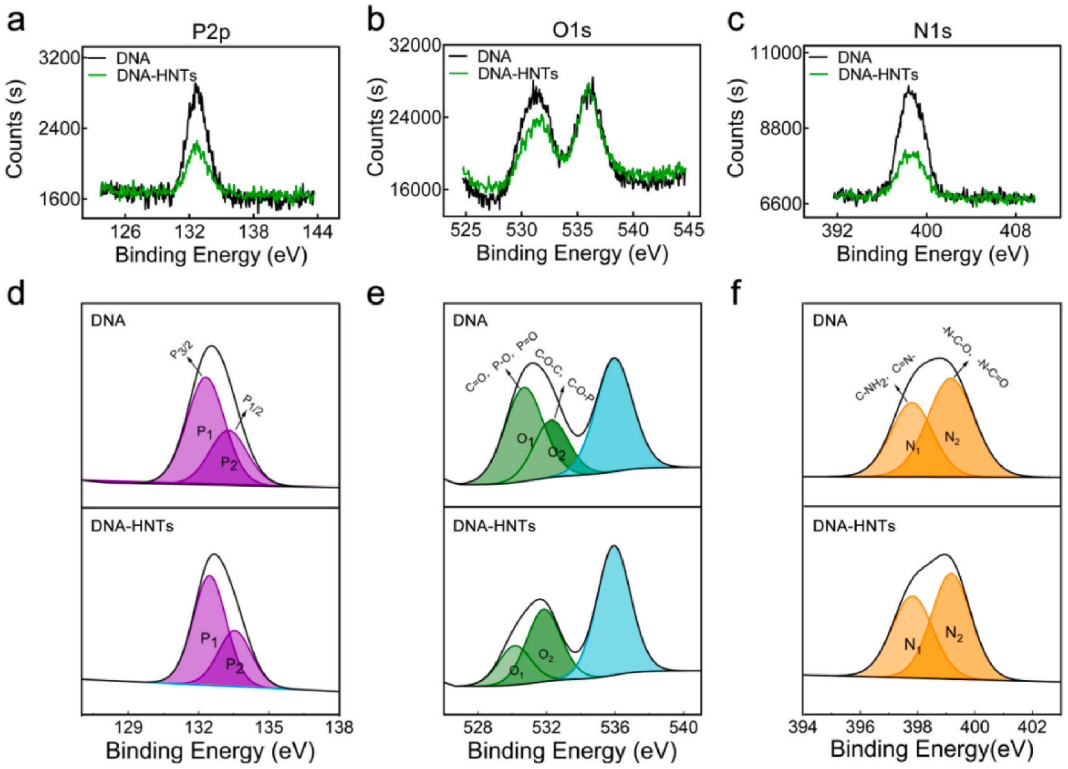

Fig. 3. XPS analysis of the DNA-based hydrogels. Comparison of high-resolution XPS spectra of DNA hydrogel and DNA-HNTs hydrogel for (a) phosphorus (P 2p), (b) oxygen (O 1s), and (c) nitrogen (N 1s). Comparison of the deconvoluted peaks of (d) P 2p, (e) O 1s, and (f) N 1s for both hydrogels to analyze the interactions between DNA and HNTs.

cells. From the drug release curves (Fig. 4a), more than 50 % of Dex was released from the DNA hydrogel after 3 days. However, the amount of Dex released from the DNA-HNTs hydrogel was much less than 50 % at the same time point, implying more retention of Dex in DNA hydrogels containing HNTs. Specifically, HNTs have a double-layer hollow tubular structure, consisting of a positively charged inner surface provided by an alumina composite (Al–OH) and a negatively charged outer surface composed of silicon dioxide (SiO_2), making negatively charged drugs, such as Dex, preferentially loaded inside the lumen. In addition, DNA-HNTs hydrogel had more compact internal structure compared with DNA hydrogel, which was more conducive to drug encapsulation. Therefore, the introduction of HNTs can effectively improve the controlled drug release performance of DNA hydrogel.

Furthermore, we evaluated the cytotoxicity of nanocomposite hydrogels, which was the basic evaluation index for implanted biomaterials [38]. The cytocompatibility of the nanocomposite hydrogels was evaluated *via* live-dead staining and Cell Counting Kit-8 (CCK-8) assay. Mouse bone marrow mesenchymal stem cells (BMSCs) were cultured in 48-well plates until cell adhesion and exposed to different nanocomposite hydrogel formulations, while the control group (ctrl) was cultured with complete medium. The live-dead staining images of BMSCs after 1, 3, and 5 days of exposure to the nanocomposite system were shown in Fig. 4b, where living cells were marked in green fluorescence and dead cells were marked in red fluorescence. The green fluorescent dots representing living cells increased significantly with increasing incubation time. BMSCs maintained good proliferation behavior without apparent dead cells, similar to the ctrl group. Consistent with the live-dead staining result, the CCK-8 assay demonstrated that the BMSCs in all groups had good proliferative viability at three preset time points, indicating good cytocompatibility of injectable DNA-based hydrogels (Fig. 4c).

In addition to good biocompatibility and controlled drug release performance, retaining the biological activity of encapsulated drugs is also one of the key properties required for hydrogel-based drug carrier materials [39]. To assess the activity of encapsulated drug, we evaluated the regulation of DNA-based hydrogels on the osteogenic differentiation behavior of BMSCs to analyze the effect of encapsulated drug Dex on the osteogenic function of BMSCs. We evaluated the effect of DNA-based hydrogels on the expression of osteogenic-related genes in BMSCs by fluorescence real-time quantitative reaction (qRT-PCR) experiment, which can speculate the biological activity of the internal osteogenic model drug Dex of DNA-HNTs hydrogel. The selected osteogenic-related genes including Runt-related transcription factor-2 (Runx-2), Alkaline phosphatase (ALP), Collagen I (Col-I), Bone sialoprotein (BSP), and Osteocalcin (OCN). The mRNA expression levels of these genes were measured at two time points, and the gene expression levels of BMSCs in the ctrl group were used for standard normalization (Fig. 4d). In the early osteogenic stage (day 7), the fold increase expression of ALP and Col-I were significantly higher in the DNA-HNTs + Dex hydrogel (32.5 ± 4.1 and 3.1 ± 0.1, respectively) and DNA-HNTs hydrogel (26.8 ± 2.4

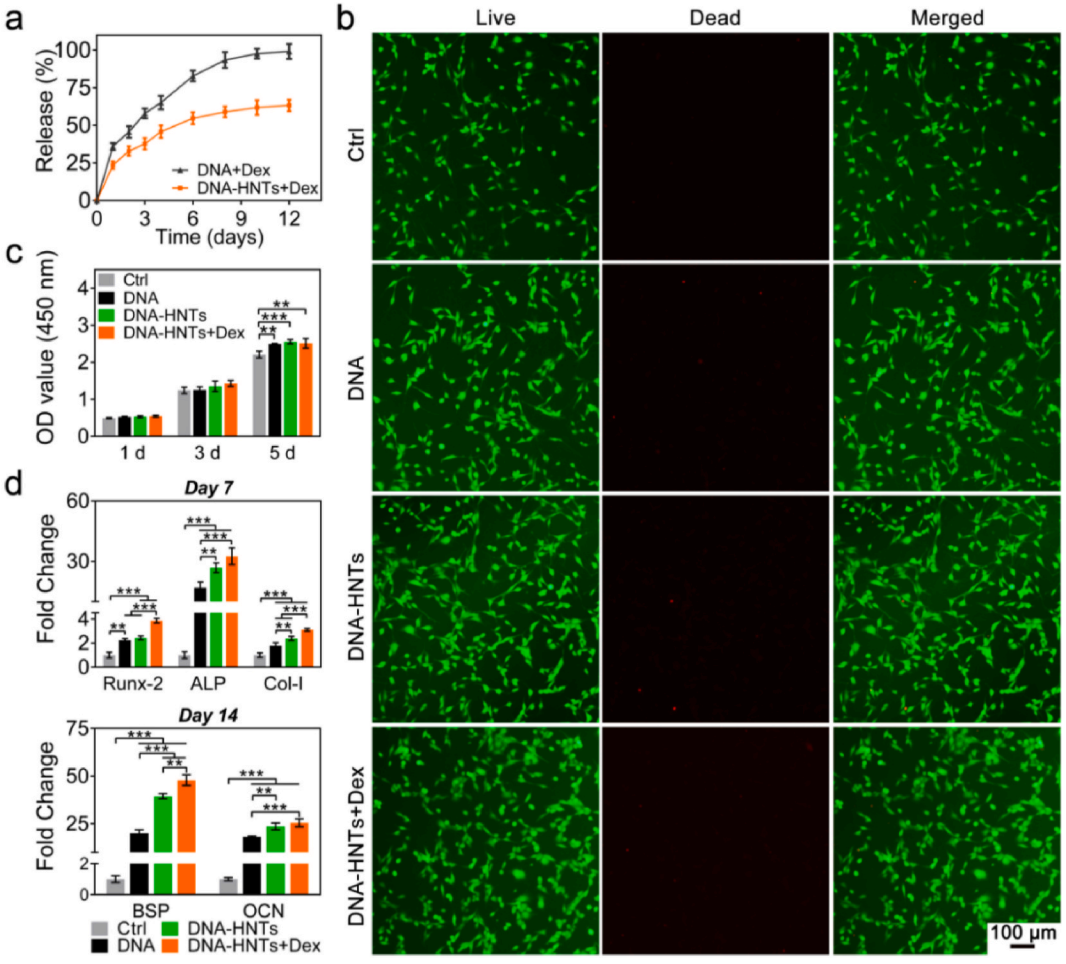

Fig. 4. (a) Release curves of Dex in a DNA-based hydrogel systems with or without HNTs. (b) Live-dead staining images of BMSCs cultured in medium containing different hydrogel formulations, and BMSCs cultured in complete medium were treated as the control group (Ctrl) (scale bar = 100 μm). (c) CCK-8 assay of BMSCs after 1, 3, and 5 days of exposure to the nanocomposite systems. (d) qPCR analysis of different osteogenic markers of BMSCs after 7 and 14 days of exposure to the nanocomposite systems. $^{*}p < 0.05$, $^{**}p < 0.01$, $^{***}p < 0.001$.

and 2.4 ± 0.2, respectively) compared to the other two groups. In the late osteogenic differentiation stage (day 14), the fold increase expression of BSP and OCN showed the highest expression level in the DNA-HNTs + Dex hydrogel, confirming that the DNA-based nanocomposite hydrogel can provided a microenvironment conducive to cellular osteogenic differentiation and effectively retain the biological activity of the encapsulated drug.

Alkaline phosphatase (ALP), as an exocrine enzyme generated in the early osteogenic differentiation process of stem cells, is closely related to the regeneration of bone tissue. The expression level of ALP can reflect the functional state of cells as well as osteogenic activity, and can be used as an important marker of cell osteogenic differentiation [40,41]. The expression levels of ALP in each groups were monitored *in vitro*. The region stained blue in the ALP staining images was the ALP secreted by the cells, and the blue area showed a significantly larger area in the DNA-HNTs + Dex hydrogel, indicating more generation of ALP (Fig. 5a). Further quantitative analysis of ALP showed that the ALP expression level of DNA-based nanocomposite hydrogel encapsulated Dex was significantly higher than those in the other groups (Fig. 5b). The formation of the mineralized matrix of BMSCs was analyzed by alizarin red staining, and the stained red region represented the mineralized matrix generated by the cells (Fig. 5c). On day 14, the red stained regions were clearly visible in hydrogel groups, especially in the DNA-HNTs and DNA-HNTs + Dex hydrogels. However, only scattered red regions were observed in the ctrl group, indicating that only a small amount of the mineralized matrix was formed in the ctrl group. Further quantitative analysis showed that the amount of mineralized matrix formed in the DNA-HNTs + Dex hydrogel group was significantly higher than that in the other groups (Fig. 5d), consistent with the results of alizarin red staining.

Overall, the constructed DNA-HNTs functionalized nanocomposite hydrogels can effectively stimulate the osteogenic differentiation of BMSCs in the absence of osteogenic induction factors. DNA-based hydrogel system was also capable of serving as a carrier system for drug molecules, such as enhancing the osteogenic activity of the hydrogel by carrying the osteogenic model drug Dex.

3.3. *In vivo* bone regeneration performance of nanocomposite hydrogel encapsulated drug

Finally, we evaluated the *in vivo* bone repair potential of DNA-based nanocomposite hydrogels in a rat cranial defect model (Fig. 6a). We set four groups *in vivo* experiment, including the material-free group (Blank) and the groups with implanted DNA, DNA-HNTs, and DNA-HNTs + Dex hydrogels. New bone regeneration in the cranial defect was observed by Micro-CT system (Fig. 6b). Compared with the blank group, there was significantly more newly formed bone after 4 and 8 weeks of hydrogel treatment, especially in the DNA-HNTs + Dex hydrogel group, where new bone mainly grew from the periphery of the defect to the central region. At the same time, there was no obvious new bone formation in the bone defect area of the blank group. The parameters of newly formed bone were further analyzed, including bone volume (BV), bone volume/tissue volume (BV/TV), and bone mineral density (BMD) (Fig. 6c–e). BV represented the volume of the newly formed bone in the defect, BV/TV represented the percentage of the volume of the newly formed bone in the total volume of the bone defect, and BMD represented the density of newly formed bone. At week 8, the BV of the DNA-HNTs hydrogel (4.08 ± 0.39 mm^3) was higher than the BV of the blank (1.58 ± 0.32 mm^3) and the DNA hydrogel (2.92 ± 0.68 mm^3). The BV of the DNA-HNTs + Dex hydrogel group (5.17 ± 0.78 mm^3) was significantly highest in these groups, indicating that DNA-based nanocomposite hydrogels can significantly promote new bone regeneration.

Further, hematoxylin and eosin (H&E) staining was used to evaluate the histological morphology of the new bone in the defect. At week 8, The H&E staining images showed a large amount of fibrous tissue in the blank group without significant newly formed bone (Fig. 7a). Meanwhile, all hydrogel groups had significantly new bone formation. This was attributed to the osteoconductive effect of the hydrogels, which was more favorable for new bone regeneration in the defect site. The H&E staining results were consistent with the Micro-CT results, suggesting that DNA-HNTs hydrogel as a drug carrier could be combined with Dex to effectively promote new bone regeneration in the defect area. As a histological staining method to label collagen fibers, masson staining can be used to analyze the generation of collagen fibers in the bone defect to evaluate the formation and maturation of bone tissue. According to the masson staining results at week 8 (Fig. 7b), the defect area in the blank group was filled with large amounts of loose connective

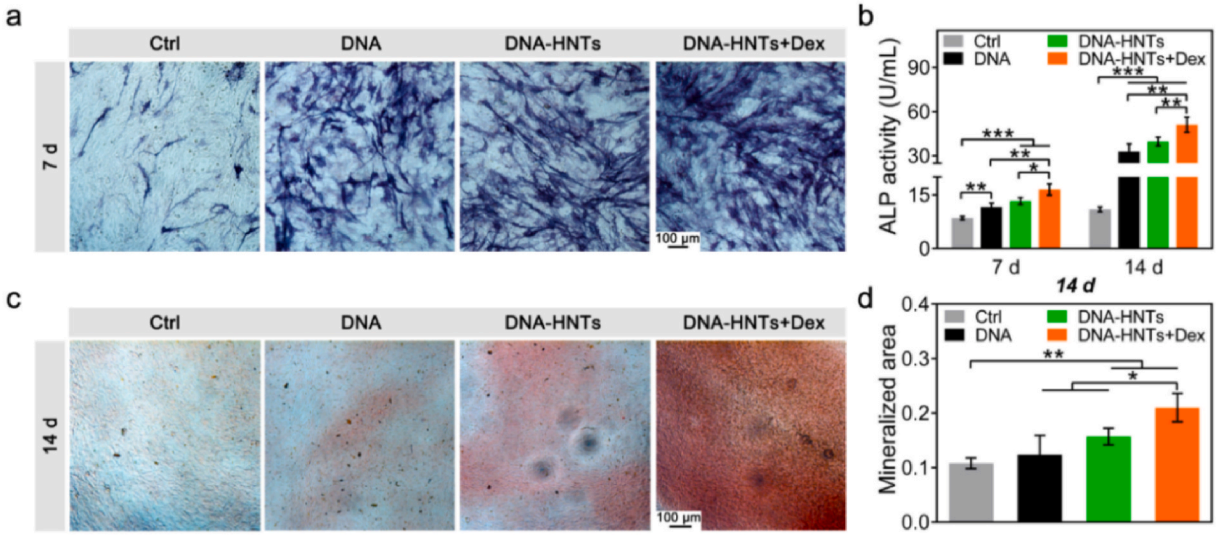

Fig. 5. (a) Images of ALP staining after BMSCs cultured in medium containing different hydrogel formulations after 7 days (scale bar = 100 μm). (b) ALP quantification indicated that the ALP expression level in the DNA-HNTs + Dex hydrogel group was significantly higher than those of the cells grown in other groups. (c) Alizarin red staining was performed on BMSCs after 14 days to detect calcium deposition (scale bar = 100 μm). (d) Quantitative analysis of calcium deposition showed that the DNA-HNTs + Dex hydrogel group significantly accelerated the formation of cellular mineralized matrix. *$p < 0.05$, **$p < 0.01$, ***$p < 0.001$. (For interpretation of the references to color in this figure legend, the reader is referred to the Web version of this article.)

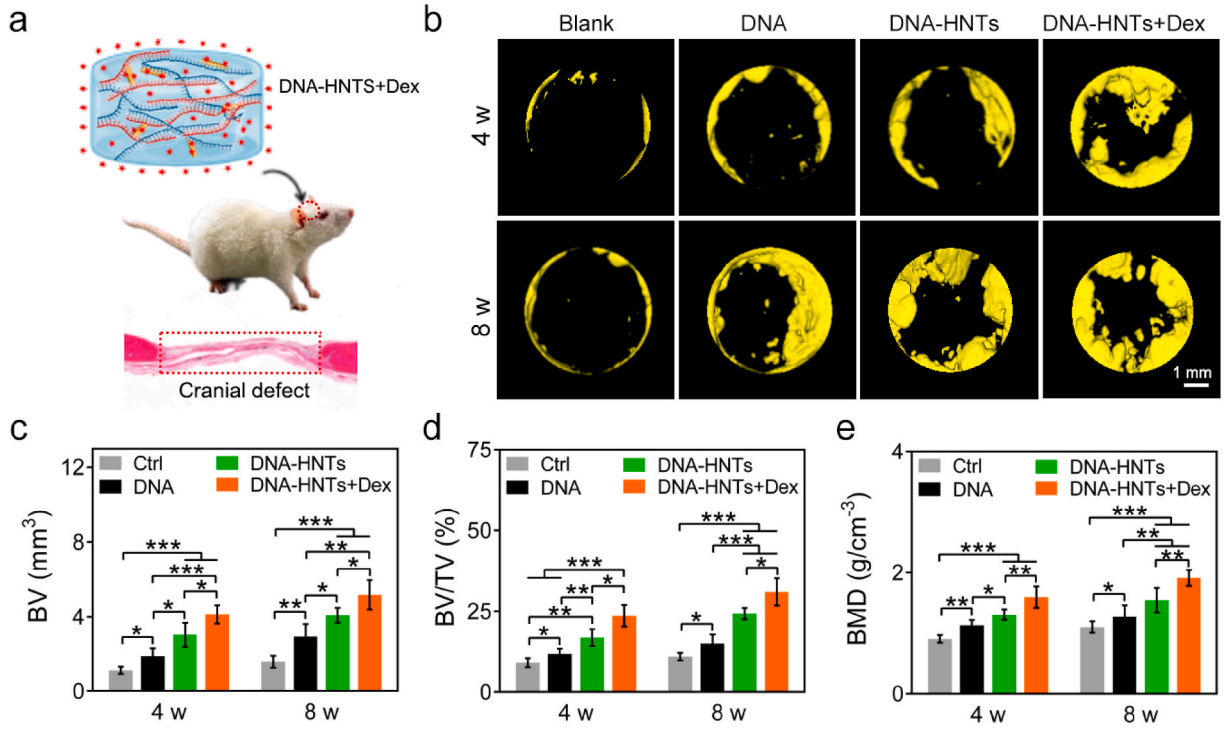

Fig. 6. (a) Schematic diagram of DNA-based hydrogel injected into rat cranial defect. (b) The newly formed bone in the cranial defect was observed through Micro-CT detection (scale bar = 1 mm). (c–e) Quantitative analysis of osteogenesis-related parameters based on Micro-CT images to analyze the effect of DNA-based hydrogels on new bone regeneration *in vivo*. $^{*}p < 0.05$, $^{**}p < 0.01$, $^{***}p < 0.001$.

tissue and without obvious collagen fiber formation, while many immature collagen fibers (blue area) could be observed in the cranial defect injected with DNA hydrogel. Compared with the other groups, more collagen fibers (blue area) and mature bone matrix (red area) were found in the DNA-HNTs hydrogel group and DNA-HNTs + Dex hydrogel group and were distributed around the hydrogels. The above results indicated that the DNA-based hydrogel containing Dex significantly promoted the repair of bone defects, and that the Dex inside the hydrogel cooperated with HNTs to promote the formation of new bone matrix.

In the process of bone matrix mineralization, osteocalcin (OCN) is mainly secreted by osteoblasts, and it is an important marker of osteogenic activity and bone formation [42], accounting for about 10%–20 % of the non-collagenous protein components of bone. Immunohistochemistry was used to evaluate the bone repair performance of DNA-based hydrogels (Fig. 7c). Compared with the bank group and DNA hydrogel group, there were obvious yellow-brown positive expression areas of OCN in DNA-HNTs hydrogel group and DNA-HNTs + Dex hydrogel group. Of these, the DNA-HNTs + Dex hydrogel group showed the pronounced positive OCN expression around the material, with a darker yellow-brown color. The HNTs and Dex inside the hydrogel synergistically enhanced the mineralization of the new bone matrix.

4. Discussions

As a natural polymer, DNA backbones treated with heating and cooling process can form a physical cross-linking network through multiple hydrogen bonds, which can serve as promising carrier to sustainably deliver active molecules including proteins and drugs [43,44]. In our study, halloysite nanotubes (HNTs) were introduced into the DNA multihydrogen bond network in order to achieve effective mechanical reinforcement and drug delivery of DNA hydrogels. Based on the analysis of zeta potential, particle size and the TEM morphology images (Fig. 1b–d), it can be speculated that there may be physical interactions between the DNA backbone and HNTs, so that HNTs were dispersed in a DNA solution without aggregation, further enhancing the dispersion stability of HNTs.

Furthermore, FTIR spectrum analysis and XPS studies validated the type of interactions between DNA and HNTs, and explored the function of HNTs in enhancing the DNA hydrogel network (Figs. 2g and 3). Specifically, it was demonstrated that there were hydrogen bond interactions and electrostatic interactions occurring between DNA and HNTs. HNTs are naturally formed by the exfoliation process of aluminosilicate minerals ($Al_2Si_2O_5(OH)_4{\cdot}nH_2O$), and have a bilayered hollow tubular structure with a positively charged inner surface afforded by alumina composition (Al–OH) and a negatively charged external surface consisting of silicon dioxide (SiO_2). The hydrogen bonding interactions mainly occurred between the amino groups of DNA and the hydroxyl groups (outer surface) of HNTs. The electrostatic interaction mainly occurred between the negatively charged phosphate groups in DNA and the positively charged regions (inner surface) of HNTs. The interactions between HNTs and DNA chain providing additional cross-linking sites for the preparation of the DNA hydrogel, synergatively regulating the mechanical stability of the hydrogel(Fig. 2c–e). The porous and hollow structures of HNTs are capable of interacting well with polymer chains and provide a strong bonding [45]. Hence, HNTs can be used as reinforcement materials in biomedical materials [32].

Additionally, HNTs exhibit a positively charged inner surface and a negatively charged external surface, making negatively charged drugs preferentially loaded inside the lumen [46], such as the osteogenic model drug dexamethasone (Dex), thus further optimizing the osteoinduction performance of DNA-HNTs hydrogels. Besides that, DNA-HNTs hydrogel had more compact internal structure compared with DNA hydrogel, which was more conducive to drug encapsulation. The experimental results also demonstrated the DNA-HNTs hydrogel enabled the effective control of Dex release (Fig. 4a). Additionally, based on the live-dead staining result and the CCK-8 assay, it can be concluded that the DNA-HNTs + Dex hydrogel had the good cytocompatibility, which met the basic evaluation index for implanted biomaterials [38].

Furthermore, analysis of the expression levels of the osteogenic

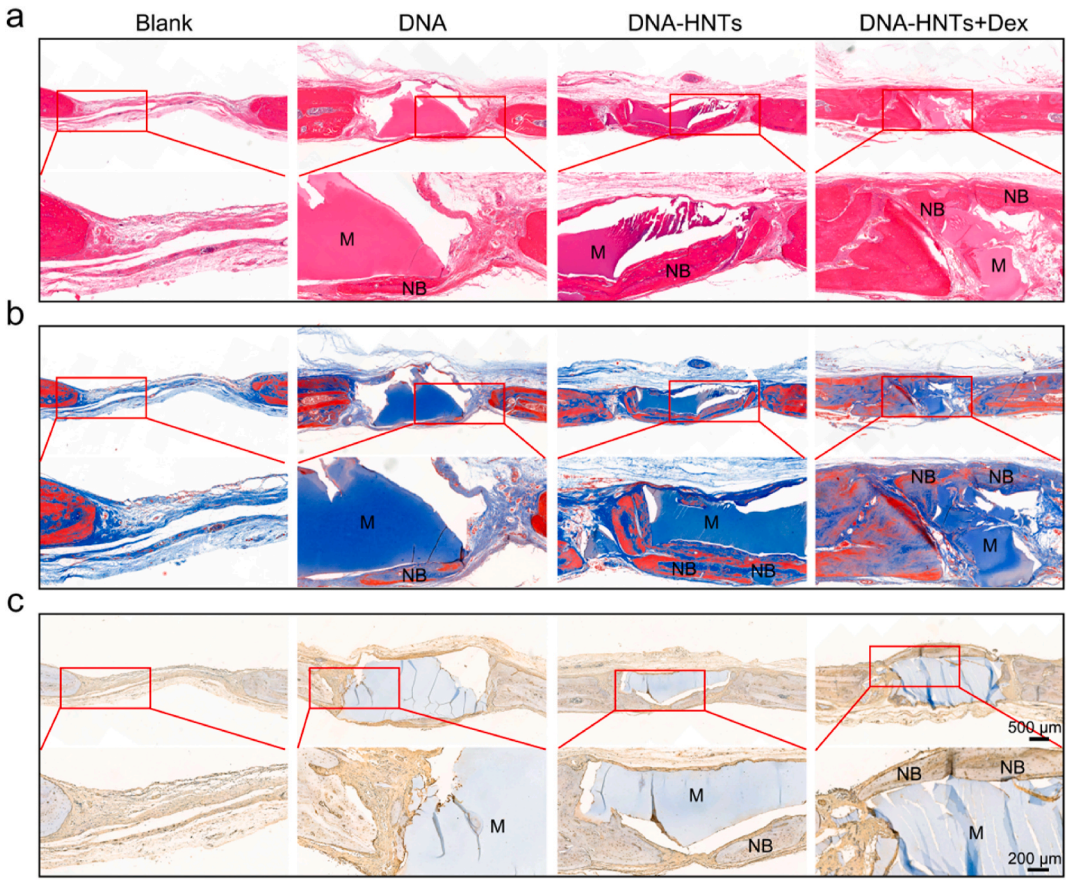

Fig. 7. (a) H&E staining images of cranial defects after the injection of hydrogels for 8 weeks. (b)Masson staining images of cranial defects after the injection of hydrogels for 8 weeks. (c) OCN immunohistochemical staining images of cranial defects after the injection of hydrogels for 8 weeks. NB stands for new bone, M stands for implant materials.

markers indicated that the DNA-based nanocomposite hydrogel favoured osteogenesis compared with DNA hydrogel, especially DNA-HNTs + Dex hydrogel, confirming that the DNA-based nanocomposite hydrogel can provided a microenvironment conducive to cellular osteogenic differentiation and effectively retain the biological activity of the encapsulated drug. Although exogenous calcium has not been introduced into HNTs, HNTs can enhance the biomineralization performance of hydrogels [47]. The combination of HNTs with hydrogel can effectively promote the osteogenic differentiation of cells [48]. Further, the possibility of DNA-based nanocomposite hydrogels as injectable bone repair materials was evaluated by cranial defect model in Sprague–Dawley rats. Based on the *in vivo* experimental relevant characterization results, it can be found that there was significantly more newly formed bone after 4 and 8 weeks of hydrogel treatment, especially in the DNA-HNTs + Dex hydrogel. The parameters of newly formed bone in the DNA-HNTs + Dex hydrogel were significantly highest in these groups, indicating that the Dex inside the hydrogel cooperated with HNTs to promote the formation of new bone matrix. The DNA-based nanocomposite hydrogel material developed in our work can be used as an injectable filling material for the repair of non-load bearing bone defect and can be loaded with osteogenic model drug dexamethasone (Dex) for improved osteoinductivity, promoting new bone regeneration *in vivo*.

It is well known that bone regeneration is a complex and long-term process involving osteogenesis and angiogenesis [49]. Since osteogenesis/angiogenesis were coupled and cytokines in angiogenesis were crucial for bone regeneration, such as PDGF and VEGF, further studies might utilize active substances to enrich the functionality of the hydrogel for osteogenesis/angiogenesis and investigate the complicated the synergenic effects of osteogenesis/angiogenesis. The tissue repair performance of DNA-HNTs + Dex hydrogel could be more efficient through this way.

In our study, the DNA-based nanocomposite hydrogels were constructed, and the potential application of the DNA-based nanocomposite hydrogels as a drug carrier material for filling and repair of non-load-bearing bone defects was investigated. Dexamethasone (Dex), which has been proven to effectively promote the osteogenic differentiation of MSCs [50,51], has been selected as the osteogenic model drug in our research. However, high doses use of Dex may indeed cause bone loss due to inhibition of inflammation, and burst release effect of Dex might trigger side effects since the metabolism of Dex is slow [52]. DNA-HNTs hydrogel as a drug carrier can effectively reduce the release rate of Dex and regulate the release amount of Dex, thus realizing the positive regulatory effect of DNA-HNTs + Dex hydrogel on the osteogenic differentiation behavior of MSCs. In addition to serving as a drug carrier material, the DNA-based nanocomposite hydrogel system may be more abundant in potential clinical applications due to its injectable extracellular matrix-like structure. For instance, the injectable hydrogel could be utilized as minimally invasive injection material for bone fracture, and as a substitute for periosteum might be another potential option. However, the clinical translation of bone regeneration biomaterials needs to undergo a long process, further studies were still need to reveal the mechanism, such as the immune regulation on macrophage polarization and the angiogenesis function of the DNA-HNTs injectable hydrogel, and this injectable hydrogel system could be utilized to obtain a multi-drug controlled release system that can regulate the osteogenic microenvironment, such as BMP2 or VEGF combined with Dex. Besides, it is also a challenge to match the degradation rate of hydrogels with tissue ingrowth rate from different position, tissue and individual.

5. Conclusion

We have successfully designed a nanocomposite hydrogel with injectable properties. Electrostatic interaction and hydrogen bonding interaction between halloysite nanotubes (HNTs) and DNA provided additional physical crosslinking sites for the hydrogel, thus effectively improving the mechanical properties of the hydrogel. The prepared nanocomposite hydrogels exhibited good biocompatibility and enabled the continuous release of the loaded model drug Dex. *In vitro* osteogenic differentiation studies confirmed that the drug retained its biological activity after release. Furthermore, DNA-based hydrogels were injected into the rat cranial defect site for *in vivo* experiments, and preliminary studies showed that DNA-based hydrogels could effectively accelerate new bone regeneration, especially in the Dex-containing hydrogel group. Taken together, these results suggested that DNA-based injectable nanocomposite hydrogels can serve as a carrier system for the model drug Dex, thus exerting a positive effect on bone repair.

Declaration of competing interest

The authors declare no conflict of interest.

Acknowledgement

This work was supported by the GuangDong Basic and Applied Basic Research Foundation (2022A1515110882), the China Postdoctoral Science Foundation (2022M720856), and the National Natural Science Foundation of China (52202358).

References

[1] Yang K, Yang J, Chen R, Dong Q, Yang H, Gu S, et al. Antibacterial hyaluronic acid hydrogels with enhanced self-healing properties via multiple dynamic bond crosslinking. Int J Biol Macromol 2023;256(Pt 2):128320.
[2] Fang Y, Huang S, Hu Q, Zhang J, King JA, Wang Y, et al. Injectable zwitterionic physical hydrogel with enhanced chemodynamic therapy and tumor microenvironment remodeling Properties for synergistic anticancer therapy. ACS Nano 2023;17(24):24883–900.
[3] Guo H, Shen H, Ma J, Wang P, Yao Z, Zhang W, et al. Versatile injectable carboxymethyl chitosan hydrogel for immediate hemostasis, robust tissue adhesion barrier, and antibacterial applications. ACS Appl Mater Inter 2023;15(45):52290–304.
[4] Dou Z, Tang H, Chen K, Li D, Ying Q, Mu Z, et al. Highly elastic and self-healing nanostructured gelatin/clay colloidal gels with osteogenic capacity for minimally invasive and customized bone regeneration. Biofabrication 2023;15(2):025001.
[5] Yu T, Hu Y, He W, Xu Y, Zhan A, Chen K, et al. An injectable and self-healing hydrogel with dual physical crosslinking for in-situ bone formation. Mater Today Bio 2023;19:100558.
[6] Bian Q, Guo C, Cui S, Liu J, Xu G, Feng W. Accelerating bone regeneration in cranial defects using an injectable organic-inorganic composite hydrogel. J Mater Chem B 2023;11(16):3713–26.
[7] Yang J, He Y, Li Z, Yang X, Gao Y, Chen M, et al. Intelligent wound dressing for simultaneous in situ detection and elimination of pathogenic bacteria. Acta Biomater 2024;174(15):177–90.
[8] Yang P, Ju Y, Liu X, Li Z, Liu H, Yang M, et al. Natural self-healing injectable hydrogels loaded with exosomes and berberine for infected wound healing. Mater Today Bio 2023;23:100875.
[9] Ge J, Fang C, Tan H, Zhan M, Gu M, Ni J, et al. Endogenous zinc-ion-triggered in situ gelation enables zn capture to reprogram benign hyperplastic prostate microenvironment and shrink prostate. Adv Mater 2023;36(11):e2307796.
[10] Lee JH, Kim PY, Pyun YC, Park J, Kang TW, Seo JS, et al. Cartilage regeneration using transforming growth factor-beta 3-loaded injectable crosslinked hyaluronic acid hydrogel. Biomater Sci 2023;12:479–94.
[11] Eivazzadeh-Keihan R, Farrokhi-Hajiabad F, Aliabadi HAM, Ziabari EZ, Geshani S, Kashtiaray A, et al. A novel magnetic nanocomposite based on alginate-tannic acid hydrogel embedded with silk fibroin with biological activity and hyperthermia application. Int J Biol Macromol 2023;224:1478–86.
[12] Sha Q, Wang Y, Zhu Z, Wang H, Qiu H, Niu W, et al. A hyaluronic acid/silk fibroin/poly-dopamine-coated biomimetic hydrogel scaffold with incorporated neurotrophin-3 for spinal cord injury repair. Acta Biomater 2023;167:219–33.
[13] Miao Y, Chen Y, Luo J, Liu X, Yang Q, Shi X, et al. Black phosphorus nanosheets-enabled DNA hydrogel integrating 3D-printed scaffold for promoting vascularized bone regeneration. Bioact Mater 2023;21:97–109.
[14] Jian G, Li D, Ying Q, Chen X, Zhai Q, Wang S, et al. Dual photo-enhanced interpenetrating network hydrogel with biophysical and biochemical signals for infected bone defect healing. Adv Healthc Mater 2023;12(25):e2300469.
[15] Guo Z, Yan L, Zhou B, Zhao P, Wang W, Dong S, et al. In situ photo-crosslinking silk fibroin based hydrogel accelerates diabetic wound healing through antibacterial and antioxidant. Int J Biol Macromol 2023;242(Pt 3):125028.
[16] Tang J, Jia X, Li Q, Cui Z, Liang A, Ke B, et al. A DNA-based hydrogel for exosome separation and biomedical applications. Proc Natl Acad Sci USA 2023;120(28):e2303822120.
[17] Ma Y, He S, Huang J. DNA hydrogels as selective biomaterials for specifically capturing DNA, protein and bacteria. Acta Biomater 2022;147:158–67.
[18] Wang Z, Li W, Gou L, Zhou Y, Peng G, Zhang J, et al. Biodegradable and antioxidant DNA hydrogel as a cytokine delivery system for diabetic wound healing. Adv Healthc Mater 2022;11(21):e2200782.
[19] Basu S, Pacelli S, Paul A. Self-healing DNA-based injectable hydrogels with reversible covalent linkages for controlled drug delivery. Acta Biomater 2020;105:159–69.
[20] Miao Y, Liu X, Luo J, Yang Q, Chen Y, Wang Y. Double-network DNA macroporous hydrogel enables aptamer-directed cell recruitment to accelerate bone healing. Adv Sci 2023;11(1):e2303637.
[21] Fadeev M, Davidson-Rozenfeld G, Li Z, Willner I. Stimuli-responsive DNA-based hydrogels on surfaces for switchable bioelectrocatalysis and controlled release of loads. ACS Appl Mater Inter 2023;15(30):37011–25.
[22] Athanasiadou D, Meshry N, Monteiro NG, Ervolino-Silva AC, Chan RL, McCulloch CA, et al. DNA hydrogels for bone regeneration. Proc Natl Acad Sci USA 2023;120(17):e2220565120.
[23] Li Y, Chen R, Zhou B, Dong Y, Liu D. Rational design of DNA hydrogels based on molecular dynamics of polymers. Adv Mater 2023;36(7):e2307129.
[24] Yang Q, Miao Y, Luo J, Chen Y, Wang Y. Amyloid fibril and clay nanosheet dual-nanoengineered DNA dynamic hydrogel for vascularized bone regeneration. ACS Nano 2023;17(17):17131–47.
[25] Zhang B, Li S, Wang Y, Wu Y, Zhang H. Halloysite nanotube-based self-healing fluorescence hydrogels in fabricating 3D cube containing UV-sensitive QR code information. J Colloid Interface Sci 2022;617:353–62.
[26] Bordini EAF, Ferreira JA, Dubey N, Ribeiro JS, de Souza Costa CA, Soares DG, et al. Injectable multifunctional drug delivery system for hard tissue regeneration under inflammatory microenvironments. ACS Appl Bio Mater 2021;4(9):6993–7006.
[27] Yavari Maroufi L, Ghorbani M. Injectable chitosan-quince seed gum hydrogels encapsulated with curcumin loaded-halloysite nanotubes designed for tissue engineering application. Int J Biol Macromol 2021;177:485–94.
[28] Karolina Pierchala M, Kadumudi FB, Mehrali M, Zsurzsan TG, Kempen PJ, Serdeczny MP, et al. Soft electronic materials with combinatorial properties generated via mussel-inspired chemistry and halloysite nanotube reinforcement. ACS Nano 2021;15(6):9531–49.
[29] Zhao P, Feng Y, Zhou Y, Tan C, Liu M. Gold@Halloysite nanotubes-chitin composite hydrogel with antibacterial and hemostatic activity for wound healing. Bioact Mater 2023;20:355–67.
[30] Xu X, Chao Y, Ma X, Zhang H, Chen J, Zhu J, et al. A photothermally antibacterial Au@Halloysite nanotubes/lignin composite hydrogel for promoting wound healing. Int J Biol Macromol 2023;258(Pt 1):128704.
[31] Dehghan-Niri M, Vasheghani-Farahani E, Eslaminejad MB, Tavakol M, Bagheri F. Preparation of gum tragacanth/poly (vinyl alcohol)/halloysite hydrogel using electron beam irradiation with potential for bone tissue engineering. Carbohydr Polym 2023;305:120548.
[32] Ghadirian S, Karbasi S. Evaluation of the effects of halloysite nanotube on polyhydroxybutyrate-chitosan electrospun scaffolds for cartilage tissue engineering applications. Int J Biol Macromol 2023;233:123651.
[33] Liu C, Xu Z, Chandrasekaran S, Liu Y, Wu M. Self-healing, antibacterial, and conductive double network hydrogel for strain sensors. Carbohydr Polym 2023;303:120468.
[34] Yao S, Zhao Y, Xu Y, Jin B, Wang M, Yu C, et al. Injectable dual-dynamic-bond cross-linked hydrogel for highly efficient infected diabetic wound healing. Adv Healthc Mater 2022;11(14):e2200516.
[35] Ribeiro JS, Bordini EAF, Ferreira JA, Mei L, Dubey N, Fenno JC, et al. Injectable MMP-responsive nanotube-modified gelatin hydrogel for dental infection ablation. ACS Appl Mater Inter 2020;12(14):16006–17.
[36] Sadeghi S, Nourmohammadi J, Ghaee A, Soleimani N. Carboxymethyl cellulose-human hair keratin hydrogel with controlled clindamycin release as antibacterial wound dressing. Int J Biol Macromol 2020;147:1239–47.
[37] Volkov IL, Smirnova A, Makarova AA, Reveguk ZV, Ramazanov RR, Usachov DY, et al. DNA with ionic, atomic, and clustered silver: an XPS study. J Phys Chem B 2017;121(11):2400–6.
[38] Liu X, Miao Y, Liang H, Diao J, Hao L, Shi Z, et al. 3D-printed bioactive ceramic scaffolds with biomimetic micro/nano-HAp surfaces mediated cell fate and promoted bone augmentation of the bone-implant interface in vivo. Bioact Mater 2022;12:120–32.
[39] Chauhan N, Gupta P, Arora L, Pal D, Singh Y. Dexamethasone-loaded, injectable pullulan-poly(ethylene glycol) hydrogels for bone tissue regeneration in chronic inflammatory conditions. Mat Sci Eng C-mater 2021;130:112463.
[40] Mostofi M, Mostofi F, Hosseini S, Alipour A, Nourany M, Hamidian R, et al. Efficient three-dimensional (3D) human bone differentiation on quercetin-functionalized isotropic nano-architecture chitinous patterns of cockroach wings. Int J Biol Macromol 2024;258(Pt 2):129155.
[41] Pizzolitto C, Scognamiglio F, Sacco P, Lipari S, Romano M, Donati I, et al. Immediate stress dissipation in dual cross-link hydrogels controls osteogenic commitment of mesenchymal stem cells. Carbohydr Polym 2023;302:120369.
[42] Wan HY, Shin RLY, Chen JCH, Assuncao M, Wang D, Nilsson SK, et al. Dextran sulfate-amplified extracellular matrix deposition promotes osteogenic differentiation of mesenchymal stem cells. Acta Biomater 2022;140:163–77.

[43] Mo F, Jiang K, Zhao D, Wang Y, Song J, Tan W. DNA hydrogel-based gene editing and drug delivery systems. Adv Drug Deliv Rev 2021;168:79–98.
[44] Zhou L, Jiao X, Liu S, Hao M, Cheng S, Zhang P, et al. Functional DNA-based hydrogel intelligent materials for biomedical applications. J Mater Chem B 2020;8(10):1991–2009.
[45] Murugesan S, Scheibel T. Copolymer/Clay nanocomposites for biomedical applications. Adv Funct Mater 2020;30(17):1908101.
[46] Veerabadran NG, Goli PL, Stewart-Clark SS, Lvov YM, Mills DK. Nanoencapsulation of stem cells within polyelectrolyte multilayer shells. Macromol Biosci 2007;7(7):877–82.
[47] Kumar A, Han SS. Enhanced mechanical, biomineralization, and cellular response of nanocomposite hydrogels by bioactive glass and halloysite nanotubes for bone tissue regeneration. Mater Sci Eng C Mater Biol Appl 2021;128:112236.
[48] Huang K, Ou Q, Xie Y, Chen X, Fang Y, Huang C, et al. Halloysite nanotube based scaffold for enhanced bone regeneration. ACS Biomater Sci Eng 2019;5(8):4037–47.
[49] Ghimire S, Miramini S, Richardson M, Mendis P, Zhang L. Role of dynamic loading on early stage of bone fracture healing. Ann Biomed Eng 2018;46(11):1768–84.
[50] Xu W, Huang W, Cai X, Dang Z, Hao L, Wang L. Dexamethasone long-term controlled release from injectable dual-network hydrogels with porous microspheres immunomodulation promotes bone regeneration. ACS Appl Mater Interfaces 2024;16(31):40581–601.
[51] Li J, Li L, Wu T, Shi K, Bei Z, Wang M, et al. An injectable thermosensitive hydrogel containing resveratrol and dexamethasone-loaded carbonated hydroxyapatite microspheres for the regeneration of osteoporotic bone defects. Small Methods 2023;8(1):2300843.
[52] Weinstein RS. Glucocorticoid-induced osteoporosis and osteonecrosis. Endocrinol Metab Clin North Am 2012;41(3):595–611.